Article

Design of Janus Nanoparticles for Mobility Control in Heterogeneous Reservoirs

Long Zang, Miaomiao Hu,* Jie Cao, Yun Cheng, Pengpeng Li, Jintang Guo,* and Hang Zhang

Read Online

ACCESS | Metrics & More | Article Recommendations

ABSTRACT: Unfavorable mobility ratios in heterogeneous reservoirs have resulted in progressively poor waterflood sweep efficiency and diminishing production. In order to address this issue, our study has developed amphiphilic-structured nanoparticles aimed at enhancing the microscopic displacement capability and oil displacement efficiency. First, the transport process of Janus nanoparticles in porous media was investigated. During the water flooding, Janus nanoparticle injection, and subsequent water flooding stages, the injection pressure increased in a "stepped" pattern, reaching 0.023, 0.029, and 0.038 MPa, respectively. Second, emulsification effects and emulsion viscosity experiments demonstrated that the amphiphilic structure improved the interaction at the oil−water interface, reducing the seepage resistance of the oil phase through emulsification. In porous media, Janus nanoparticles transported with water exhibit 'self-seeking oil' behavior and interact with the oil phase, reducing the viscosity of the oil phase from 19 to 5 mPa·s at 80 °C. Finally, the core model

displacement experiment verified the characteristics of Janus nanoparticles in improving the oil−water mobility ratio. Compared with the water flooding stage, the recovery percent increased by 20.8%, of which 13.7% was attributed to the subsequent water flooding stage. Utilizing the asymmetry of the Janus particle structure can provide an effective path to enhanced oil recovery in inhomogeneous reservoirs.
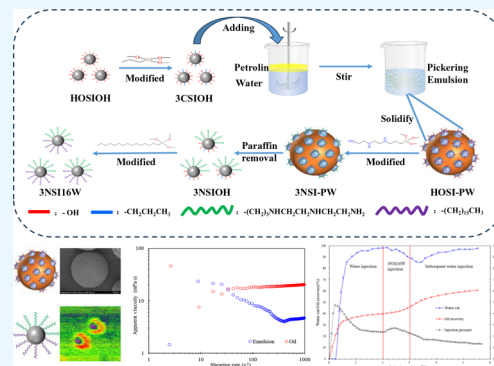
1. INTRODUCTION

With the deepening development of reservoirs, oil fields are entering a high-water-cut phase, marked by significant changes in reservoir heterogeneity and a notable decline in well productivity.[1] Prolonged water injection has notably altered the macro and microstructure of reservoir rocks, exacerbating water channeling phenomena in high-permeability layers and large pores, thereby diminishing water-flooding recovery rates.[2,3] Therefore, employing advanced techniques is crucial to boosting recovery rates and significantly increasing oil field productivity.

In recent years, the application of nanotechnology in enhancing petroleum recovery has emerged as a highly promising technology. Nanoparticles, characterized by their small particle size and a large surface-area-to-volume ratio, exhibit exceptional interfacial adsorption properties.[4,5] They demonstrate remarkable stability under high-temperature and high-salinity conditions, making them particularly useful in the pursuit of increased petroleum recovery. Bila and Torsæter have demonstrated through oil displacement experiments that polymer-encapsulated nano silica particles can improve oil recovery by up to 6% of the original oil in place.[6] Pereira et al., through experimentation, observed that the synergistic interaction between Fe_3O_4 nanofluid and cationic surfactant CTAB effectively enhanced rock wettability, ultimately leading to a

substantial increase in oil recovery rates of up to 60%.[7] Ehtesabi et al. discovered through experiments that rutile and amorphous titanium dioxide can enhance oil recovery by modifying the wettability of rocks, resulting in a 31% increase compared to water flooding.[8] Nanoparticles primarily enhance oil recovery by modifying rock wettability, reducing interfacial tension, forming microemulsions, and mitigating the wedging effect.[9−11]

However, conventional homogeneous nanoparticles lack strong interfacial activity and the ability to form emulsions that remain stable over an extended period.[12,13] To address the suboptimal interfacial performance of homogeneous nanoparticles, Janus nanoparticles have been extensively studied recently. Janus nanoparticles have asymmetric structures or properties, often referred to as "colloidal surfactants", which provide superior interfacial stability compared to homogeneous particles. Tang et al. experimentally demonstrated that Janus nano-SiO_2 dispersions can reduce the interfacial tension
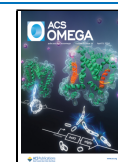
between crude oil and water to the order of 10^{-2} mN/m. 0.05% concentration of Janus nano-SiO_2 dispersions can improve recovery by 14.6% on a water-driven basis under the conditions of 65 °C and 8000 mg/L mineralization.[14] Janus nanoparticles have a strong ability to reduce interfacial tension, which in turn enhances oil recovery.

Now, there is a gap in the study of Janus nanoparticles in modulating the mobility difference of water drives in different pore channels and in modifying the oil−water flow ratio. In order to fill this gap, we prepared a modified SiO_2 with an asymmetric structure using the Pickering emulsion interfacial protection method. The structural characterization and validation of these Janus nanoparticles were conducted using scanning electron microscopy (SEM), infrared spectroscopy (FTIR), thermogravimetric analysis (TGA), Kelvin probe force microscopy (KPFM), zeta potential measurements, and contact angle measurements. Conducting flow resistance experiments to investigate its permeability characteristics in porous media and employing core model displacement experiments, self-migration experiments, and emulsification experiments to explore its ability to modify the oil−water mobility ratio.

2. EXPERIMENTAL SECTION

2.1. Material. Reagent-grade tetraethyl orthosilicate (TEOS) was provided by Shanghai Aladdin Bio-Chem Technology Co., Ltd. Analytical-grade anhydrous ethanol was supplied by Tianjin Yuanli Chemical Co., Ltd. Ammonia solution (25%) was provided by Kaimate Chemical Technology Co., Ltd. Propyltrimethoxysilane(KH-313) was obtained from Shanghai Aladdin Bio-Chem Technology Co., Ltd. Trimethoxysilyl Propyl Diethylenetriamine (DET3) was also provided by Shanghai Aladdin Bio-Chem Technology Co., Ltd. Hexadecyltrimethoxysilane(KH-1631) was supplied by Tianjin Xiensiaopei Technology Co., Ltd. The paraffin wax with a melting point between 58 and 60 °C was provided by Tianjin Yuanli Chemical Co., Ltd. Distilled water was prepared in the laboratory using a distillation apparatus. 100cs silicone oil was provided by Huahui Chemical. The rock core used in this study was synthetic, and Table 1 provides the rock's properties. The viscosity properties of the crude oil used in this study can be found in Figure 13b.

Table 1. Physical Properties of Artificial Rock Cores

rock core samples	length (cm)	diameter (cm)	pore volume (cm^3)	porosity (%)	permeability (mD)
1	30	2.5	39.7	27	145.2
2	30.4	2.5	40.6	28	155.5

2.2. Preparation of Janus-SiO_2. Janus-SiO_2 is synthesized using the Pickering emulsion interface protection method (Figure 1).[15]

Initially, nano-SiO_2 (HOSIOH) was prepared by the sol−gel method.[16] TEOS (29.4 g), anhydrous ethanol (258.7 g), and distilled water (23.7 g) were placed in a three-necked flask, and ammonia was added to adjust the pH of the system to 9, and the reaction was carried out at 25 °C for 20 h. Then the temperature was raised to 50 °C, a trace amount of KH-313 (0.02 g) was added, and the reaction was carried out for 20 h. Micromodified nano-SiO_2 (3CSIOH) was produced.

Subsequently, a Pickering emulsion was prepared by homogenizing and stirring sliced paraffin (5 g), water (50 g), 3CSIOH (1 g), and sodium chloride (0.05 g) for 5 min at 70 °C

and 8000 rpm. After cooling, the mixture was filtered and washed to obtain nanosized SiO_2-coated paraffin-structured particles (HOSI-PW), which are called "strawberry particles" because of their resemblance to strawberry particles.

Finally, anhydrous ethanol was used as a solvent, dried strawberry particles (12 wt %) and water were added to ethanol, then the pH of the system was adjusted to 9, the modifier DET3 (3 wt %) was added, and the reaction was carried out for 20 h at 50 °C. The product was centrifuged, removed paraffin, and then dried to obtain 3NSIOH. Continuing with anhydrous ethanol as solvent, 3NSIOH (10 wt %) and water were added to ethanol, then the pH of the system was adjusted to 9. The modifier KH-1613 (0.2 wt %) was added, and the reaction was carried out for 20 h at 50 °C. After separation, washing, and drying, Janus-SiO_2 nanoparticles (3NSI16W) are obtained.

2.3. Structural Characterization of Nanoparticles.
2.3.1. Scanning Electron Microscopy (SEM) Characterization. The sample powder is evenly spread onto double-sided carbon conductive tape, which is then affixed to the sample holder. Following sputter-coating with gold, the sample is examined using a field-emission scanning electron microscope (Regulus 8100) to analyze the microstructure and morphology of various SiO_2-based nanoparticles.

2.3.2. Infrared Spectroscopy Characterization. The samples are prepared using the KBr pellet method, and the scanning range is set from 400 to 4000 cm^{-1}. Fourier transform infrared spectroscopy (FT-IR) measurements of various SiO_2-based nanoparticles are carried out by using an iS50 FT-IR spectrometer at room temperature.

2.3.3. Thermal Analysis Characterization. The thermal decomposition processes of various SiO_2-based nanoparticles are analyzed by using thermal gravimetric analysis (TGA) obtained with a simultaneous thermal analyzer (STD-1600HT). The TGA is conducted at a scanning rate of 10 °C/min under a nitrogen atmosphere, ranging from 40 to 800 °C.

2.3.4. KPFM and Zeta Potential Characterization. A dispersion of 3NSI16W (0.001 wt %) in ethanol is spin-coated onto a silicon wafer. The silicon wafer is electrically connected to a conductive silver paste on both the top and bottom, allowing for conduction through the iron plates. After drying, KPFM images are obtained using a Bruker Dimension ICON AFM operated in peak force KPFM mode. Nanoscope analysis software is utilized to process the KPFM images.[17] Additionally, the ζ-potential of water dispersions of various SiO_2-based nanoparticles is measured by using a nanoparticle size and zeta potential analyzer (Zetasizer Nano ZS).

2.3.5. Contact Angle Characterization. The 0.1 wt % sample ethanol dispersion was applied onto the surface of a glass slide and allowed to dry, and this process was repeated 3−5 times until a white film formed on the glass slide surface. The contact angle of the sample was measured using a contact angle measurement instrument (CA200S).

2.4. Application Characterization of Nanoparticles. As mature water-flooded oilfields enter the high-water-cut development phase with significant heterogeneity, achieving optimal oil recovery is largely contingent on controlling the sweep and displacement factors.[18,19] Therefore, this study examines flow resistance (which impacts sweep efficiency) and displacement performance (which influences oil recovery efficiency).

2.4.1. Self-Aggregation Analysis of 3NSI16W Particles. The particle size of a 0.05 wt % concentration of 3NSI16W water dispersion was measured using a nanoparticle size and a zeta potential analyzer (Zetasizer Nano ZS). The morphology of
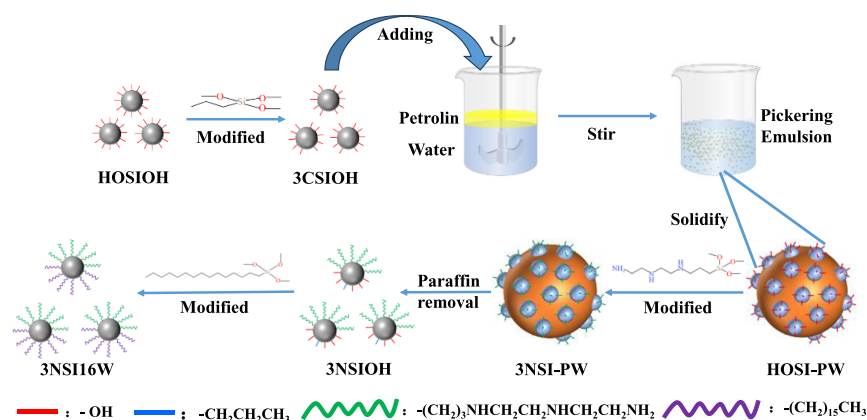
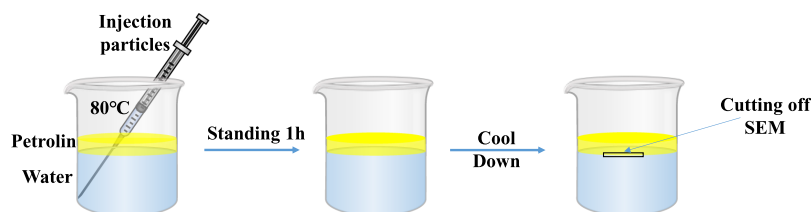**Figure 1.** Preparation flowchart of Janus-SiO$_2$.

Figure 2. Microscopic self-migration experiment.

3NSI16W particles was captured in the water dispersion by utilizing a field emission transmission electron microscope (JEM-2100F).

2.4.2. Analysis of the Flow Behavior of 3NSI16W Particles in Porous Media. Experimental studies were conducted by using a sand-packed tube displacement model. The experimental setup utilized a sand-packed tube measuring 30 cm × 2.5 cm, filled with 80−100 mesh quartz sand. A sand-packed tube (sample 1 from Table 1) was prepared, and its mass was measured. After the sample was saturated with water, the mass was measured again. The difference in mass before and after saturation was utilized to calculate the porosity of the sand-packed simulated core. Finally, water flooding, 3NSI16W aqueous dispersion flooding (0.05 wt %), and subsequent water flooding were carried out under simulated reservoir conditions at 80 °C, and the injection pressure was recorded to calculate the stabilized plugging efficiency.

2.4.3. Analysis of the Self-Seeking Ability of 3NSI16W Particles. Macro-dispersion experiment: first, 0.1 g of HOSIOH, 3NSI16W, and 16WSI16W (hydrophobic nano-SiO$_2$ obtained by symmetric modification with the same amount of KH-1613) were placed at the bottom of three measuring cylinders, then 5 g of deionized water and 5 g of silicone oil were added into the cylinders sequentially, and finally, the dispersion of nanoparticles in the oil−water system was observed.

Microscopic self-migration experiment (Figure 2) is described below:

First, 50 g of deionized water and 5 g of sliced paraffin were added into a beaker at 80 °C. When the sliced paraffin melted, 1 g of the 3NSI16W dispersion was injected into the bottom of the beaker using a syringe and left to stand for 1 h. Finally, the system was cooled so that the paraffin solidified, and the solidified paraffin slices were taken to be photographed for their morphology using a scanning electron microscope (S4800).

2.4.4. Emulsification Performance of 3NSI16W Particles. Three portions of silicone oil (6 g each) were added to aqueous

dispersions of HOSIOH, 3NSI16W, and 16WSI16W (14 g each at 0.05 wt %) to obtain three mixture systems. Emulsions were prepared by continuously shaking the mixture up and down for 30 s. Subsequently, these emulsions were aged for 7 days, and images were captured to assess the emulsification results. The emulsification index (EI) was employed to evaluate the stability of the emulsions.

$$EI = \frac{V_e}{V_0} \times 100\%$$

where V_e represents the volume of the stable emulsion and V_0 is the total system volume.[20]

Silicone oil was employed as the oil phase, and 3NSI16W (0.05 wt %) aqueous dispersions with salt concentrations of 0 10, 30, and 50,000 ppm were used as aqueous phases. The water-to-oil mass ratio was maintained at 3:7. Emulsions were generated by continuously shaking the mixture up and down for 30 s. Subsequently, these emulsions were aged for 14 days, and images were captured to assess the emulsification results. The size of emulsion droplets was observed by using an Olympus BX43 microscope, and emulsion stability was evaluated by using the Emulsification Index (EI).

The rheological properties of the emulsion were measured using a HAAKE Viscotester IQ Air (Thermo Electron, Germany), equipped with a four-blade rotor and a Peltier temperature control system. The rotor and sample cup had diameters of 22 and 25 mm, respectively. Before conducting rheological measurements, emulsions stabilized by 3NSI16W particles were prepared using crude oil as the oil phase at 80 °C. Subsequently, apparent viscosities (η) of the emulsions stabilized by 3NSI16W particles were measured at shear rates (ξ) ranging from 1 to 1000 s^{-1} at temperatures of 80, 50, and 20 °C. Additionally, the apparent viscosity (η) of the crude oil was measured at 80 °C.

2.4.5. Displacement Efficiency of 3NSI16W Particles. Experimental studies were conducted using a sand-packed
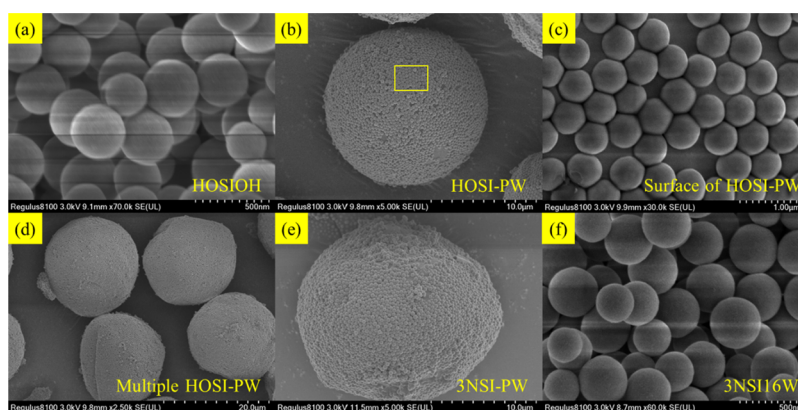
Figure 3. Morphologies of various particles obtained through the preparation process: (a) HOSIOH; (b) HOSI-PW; (c) surface of HOSI-PW; (d) multiple HOSI-PW; (e) 3NSI-PW; and (f) 3NSI16W.

tube displacement model. The experimental setup employed a sand-packed tube measuring 30 cm × 2.5 cm, filled with 80−100 mesh quartz sand. A simulated core (sample 2 from Table 1) was prepared, and the core's air permeability and porosity were measured. The core was placed in a core holder and saturated with oil at 80 °C, establishing residual water saturation. Water flooding was then initiated until the produced liquid reached 98% water content and the water flooding recovery was calculated. After the water flooding phase, 1 pore volume (PV) of ultrasound-treated 3NSI16W particle dispersion (concentration: 0.05 wt %) was injected. Finally, water injection was resumed until the produced liquid reached 98% water content and the ultimate recovery was calculated.

3. RESULT AND DISCUSSION

3.1. Physical Property and Structure of Nanoparticles.

3.1.1. Scanning Electron Microscopy. Microscopic morphologies of HOSIOH, HOSI-PW, 3NSI-PW, and 3NSI16W are listed in Figure 3. Figure 3a illustrates the morphology of HOSIOH, indicating that the nanoscale SiO_2 obtained through the sol−gel method is spherical, with particle sizes ranging from 200 to 300 nm. In Figure 3b, microscale particles of HOSI-PW, approximately 15 μm in size, are prepared using the Pickering emulsion template method. When zoomed in, as shown in Figure 3c, it can be observed that nanoscale SiO_2 uniformly coats the surface of HOSI-PW, forming a single layer that encapsulates the paraffin core. This uniform covering is advantageous for ensuring effective modification of the majority of particles, thereby enhancing the efficiency of Janus particle preparation. Figure 3d demonstrates that all of the HOSI-PW particles are uniformly covered with a single layer of nanoscale SiO_2. Figure 3e displays the morphology of 3NSI-PW, with particles maintaining their premodification appearance, and only a small fraction of nanoscale SiO_2 appears to have detached, confirming the successful protection of the nanoscale SiO_2. Finally, Figure 3f depicts the morphology of the end product, 3NSI16W, which, compared with HOSIOH, retains its spherical structure, with no significant change in the particle size.

3.1.2. FTIR Spectroscopy. The FTIR spectra of HOSIOH and 3NSI16W are depicted in Figure 4. In HOSIOH, the broad peak at 3410 cm^{-1} corresponds to the stretching vibrations of H−O−H in adsorbed water on the silicon surface and the Si−OH groups of silicon hydroxide. The peak at 1100 cm^{-1} is attributed to the asymmetric stretching vibrations of the Si−O−Si bonds. The characteristic absorption peak at 960 cm^{-1} arises from the
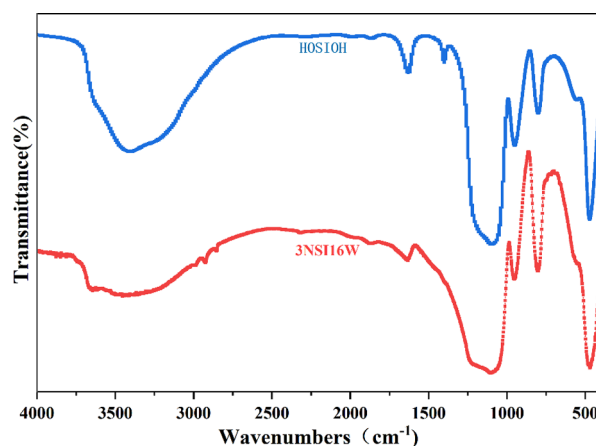

Figure 4. Infrared spectra of HOSIOH and 3NSI16W.

stretching vibrations of Si−OH, while the peak at 798 cm^{-1} is induced by the symmetric stretching vibrations of Si−O−Si bonds. These distinct peaks confirm the presence of silicon dioxide, indicating the successful synthesis of silanol-rich nano SiO_2 through the sol−gel method.[21] In comparison to HOSIOH, 3NSI16W exhibits a dual peak at 3410 cm^{-1}, providing evidence for the presence of amino groups and the grafting of DET3. The characteristic absorption peaks at 2930 and 2850 cm^{-1} arise from the −CH_2 and −CH_3 groups in both DET3 and KH-1631.[22] This observation underscores the successful modification of 3NSI16W with DET3 and KH-1631.

3.1.3. TG/DTG Curves. To further demonstrate the presence of amino groups and thereby confirm the successful grafting of diethylenetriamine, thermal weight loss curves for HOSIOH, 3NSIOH, and 3NSI16W were analyzed. HOSIOH exhibits two decomposition stages: the weight loss between 40 and 190 °C is attributed to the evaporation of physically adsorbed water and the loss of chemically adsorbed water,[23] while the weight loss at 470 °C is due to the abundance of silanol groups on the surface of nanoscale SiO_2. In comparison to HOSIOH, 3NSIOH shows two additional decomposition stages (Figure 5). The weight loss between 210 and 270 °C is attributed to the decomposition of primary amines on the diethylenetriamine propyl groups, while the weight loss between 320 and 390 °C is attributed to the decomposition of secondary amine groups on the diethylenetriamine propyl groups and the degradation of the hydrocarbon main chain.[24] For 3NSI16W, the peak of the final decomposition stage is larger than that of 3NSIOH. This is because the
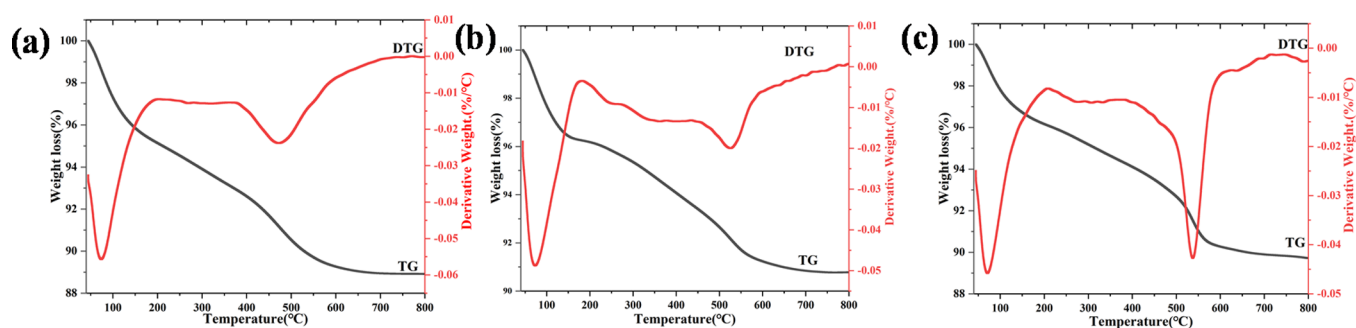
Figure 5. Thermal decomposition of prepared Janus particles and intermediates: (a) HOSIOH, (b) 3NSIOH, and (c) 3NSI16W.
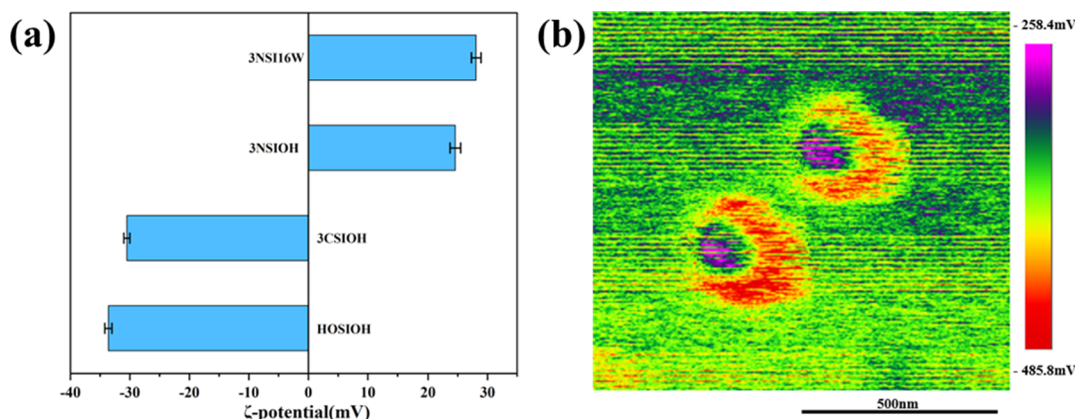

Figure 6. (a) ζ-potential of particles modified with nanosized SiO_2. (b) KPFM image of 3NSI16W.

hexadecyl groups grafted onto 3NSI16W also decompose in this stage. The grafting groups of 3NSI16W begin to decompose at around 200 °C, and its excellent high-temperature resistance makes it remain stable in ultrahigh-temperature reservoirs (150−180 °C).

3.1.4. Zeta Potential and KPFM. In Figure 6a, the ζ-potential values of particles modified with nanosized SiO_2 are presented. The ζ-potential of HOSIOH is −33.6 mV, primarily attributed to the numerous silanol groups exposed on the surface of bare nanosized SiO_2. 3CSIOH exhibits a ζ-potential of −30.5 mV, which is slightly higher than that of HOSIOH, due to the partial substitution of silanol groups by a propyl group. The ζ-potential of 3NSIOH is 24.6 mV, a result of the partial substitution of silanol groups by DET3 groups carrying three amino groups.[25,26] Finally, 3NSI16W exhibits a ζ-potential of 28.1 mV, indicating the partial substitution of silanol groups by hexadecyl groups.

Figure 6b illustrates the surface charge distribution of 3NSI16W. While the potential on the Si chip is approximately constant, the surface potential distribution on 3NSI16W is uneven, with most of the 3NSI16W showing a strong negative charge, indicated by the red color. A portion of the top surface exhibits a weaker negative charge, as shown in purple, attributed to the grafting of DET3 groups. The uneven surface potential distribution of the particles suggests that the synthesized 3NSI16W exhibits an amphiphilic structure.

3.1.5. Contact Angle. Figure 7 depicts the wettability of five particle types: HOSIOH, 3CSIOH, 3NSIOH, 3NSI16W, and 16WSI16W. HOSIOH exhibits a water contact angle of 0°, indicating a super hydrophilic structure. Due to this structure, HOSIOH cannot produce stable Pickering emulsions and tends to prefer the aqueous phase rather than the oil−water interface. After minor hydrophobic modification, the contact angle of
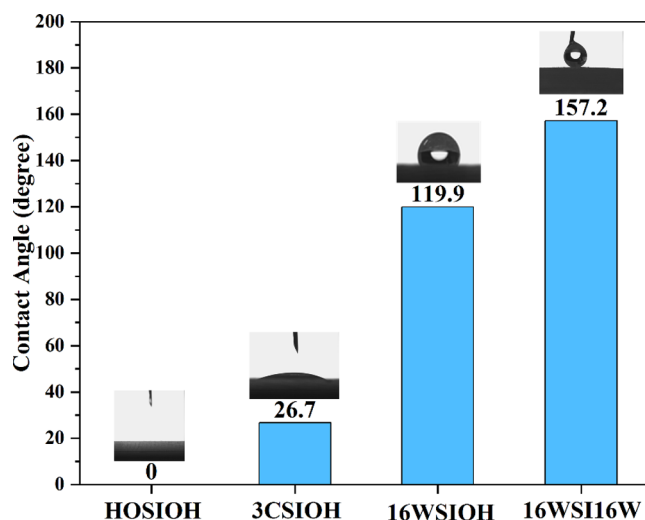

Figure 7. Contact angles of prepared Janus particles and intermediates.

3CSIOH with water increased to 28.8°, signifying reduced water affinity and improved stability in forming Pickering emulsions. With the introduction of DET3, 3NSIOH achieves a remarkable reduction in its water contact angle, measuring only 4.5°, a significant decrease compared to 3CSIOH's 28.8°. This demonstrates that one end of 3NSIOH, grafted with DET3, possesses exceptionally strong hydrophilic properties. When particles are partially wetted by water or oil (typically in the range of 50−130°), stable Pickering emulsions can be formed.[27] 3NSI16W has a contact angle of 66.3° with water, making it more prone to stability at the oil−water interface compared to HOSIOH and 16WSI16W.
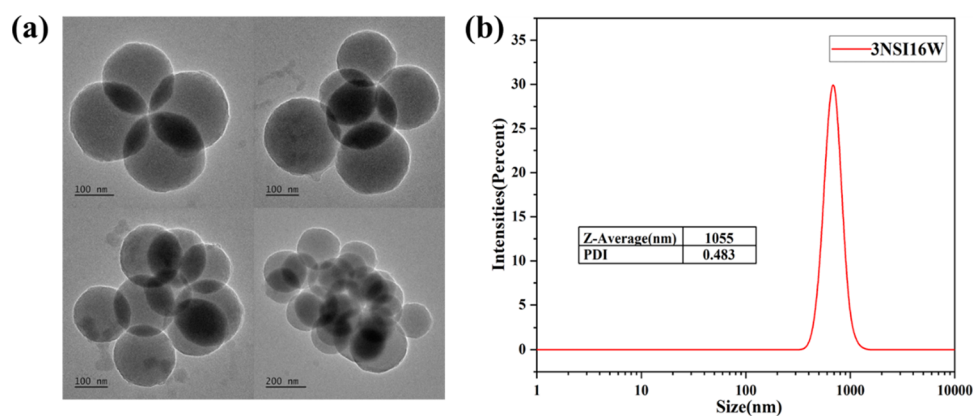
Figure 8. Particle size distribution of 3NSI16W particle dispersions: (a) TEM diagram of 3NSI16W; (b) particle size distribution of 3NSI16W.
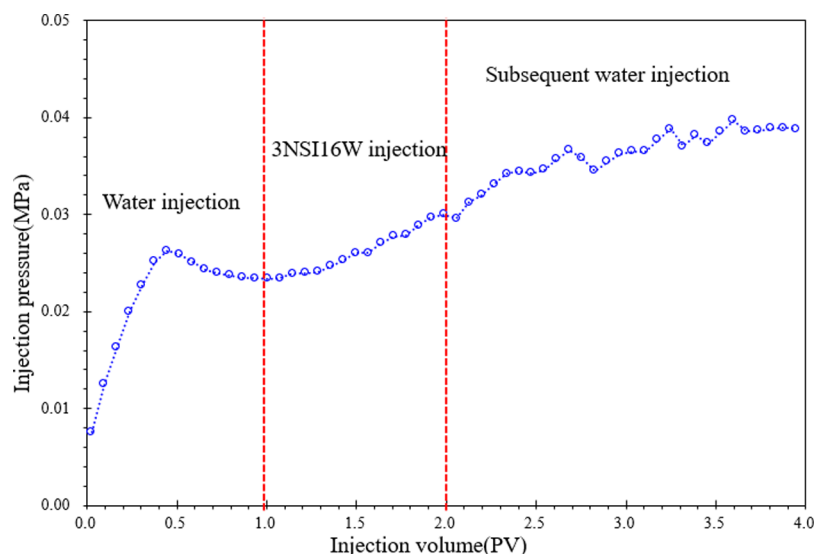

Figure 9. Flow behavior of 3NSI16W particles in porous media.

3.2. Sealing Performance and the Working Mechanism. *3.2.1. Self Aggregation of 3NSI16W Particles.* Figure 8 displays the particle size distribution of the 3NSI16W particles dispersed in water. As shown in Figure 8a, the 3NSI16W particles exhibit a propensity for self-aggregation, forming aggregates of varying sizes in water. This aggregation is driven by hydrogen bonding interactions between the hydrophilic ends of the particles and their high surface energy and is reversible. In Figure 8b, it is evident that the aggregate sizes range from 400 to 1280 nm. This range aligns with the nano/microscale pore throats in sandstone reservoirs,[28] indicating that 3NSI16W particles possess effective water-blocking abilities, enhancing flow resistance and improving sweep efficiency. Furthermore, since this aggregation is reversible, shear forces can induce dispersion, facilitating continued transport.

3.2.2. Flow Behavior of 3NSI16W Particles in Porous Media. Figure 9 shows the permeability characteristics of Janus particles in porous media. The primary water flooding pressure gradually increased to 0.026 MPa until breakthrough and then stabilized at 0.023 MPa. This is because as water enters the porous medium of the rock, its compressibility increases, and the pressure builds gradually rather than reaching an immediate peak to achieve a breakthrough. After breakthrough, the compressibility of water decreases, until it reaches a stable value.

Upon injecting 3NSI16W particles, the pressure slowly increased from 0.023 to 0.03 MPa. This is attributed to the progressive migration of 3NSI16W particles in the pore channels, which increases the flow resistance. The secondary water flooding pressure exhibited fluctuating increases, ultimately reaching 0.039 MPa, which is higher than the pressure during the injection of 3NSI16W particles. This is because during the injection of 3NSI16W particles, most of the particles are located in the front section of the core, which experiences a significant pressure gradient, allowing even a slight pressure increase to move particles near the wellbore.

During secondary water flooding, most particles migrate to the middle section of the core, where the pressure gradient is much smaller. The sealing capacity of particle clusters in this section effectively accumulates, requiring a higher pressure to displace them. Due to the shear dispersion capability of particle clusters, some clusters undergo shear dispersion, leading to a decrease in flow resistance. Consequently, the pressure does not exhibit a steady increase but shows some fluctuations.

Through calculations based on the injection pressure during primary water flooding, 3NSI16W particle flooding, and secondary water flooding when the pressure stabilizes, a resistance coefficient of 1.276 and a residual resistance coefficient of 1.555 can be determined. These data confirm that the 3NSI16W particles are effective in blocking pore
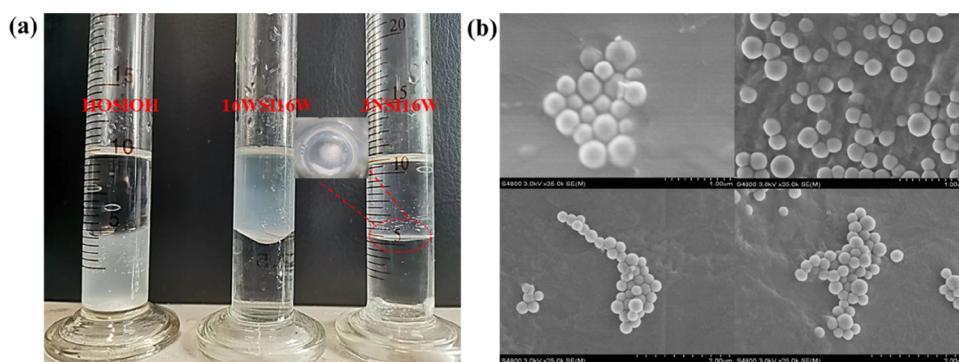
Figure 10. (a) Macroscopic dispersion experiment results for 3NSI16W. (b) Microscopic self-migration experiment results for 3NSI16W
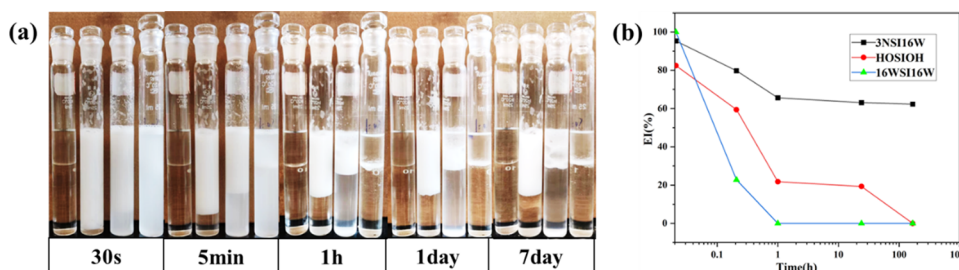

Figure 11. (a) Changes in emulsions stabilized by 3NSI16W, HOSIOH, and 16WSI16W particles after 7 days of aging, ordered from the left to right (with the first being the oil—water reference sample). (b) Variations in the EI over time for 3NSI16W, HOSIOH, and 16WSI16W particles.
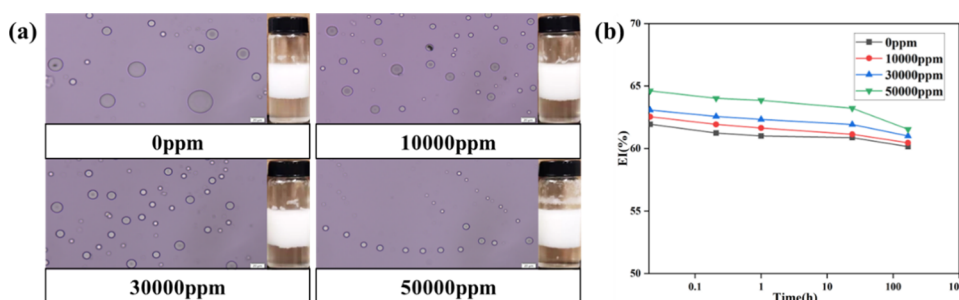

Figure 12. (a) Photos of stable emulsions of 3NSI16W particles aged for 7 days at different salt concentrations along with particle size images. (b) Evolution of the emulsion instability (EI) over time for 3NSI16W particles in stable emulsions at various salt concentrations.

throats, increasing the flow resistance of water, and thereby enhancing the sweep efficiency of waterflooding

3.3. Displacement Performance and Mechanism Analysis.
3.3.1. Self Migration Behavior of 3NSI16W Particles.
To confirm the self-seeking oil properties of 3NSI16W, macroscopic dispersion experiments and microscopic self-migration experiments were conducted. As seen in Figure 10a, in the oil—water system, HOSIOH particles disperse in the aqueous phase, 16WSI16W particles disperse in the silicone oil, and 3NSI16W particles are positioned at the oil—water interface. This is attributed to the hydrophilicity of the HOSIOH particles, the lipophilicity of the 16WSI16W particles, and the amphiphilic nature of the 3NSI16W particles. From a macroscopic perspective, 3NSI16W particles tend to reside at the oil—water interface. Figure 10b demonstrates the presence of abundant aggregates of 3NSI16W particles on the surface of the solidified wax blocks. This microscopically illustrates the capability of 3NSI16W particles to self-migrate from the aqueous phase to the oil—water interface. Following injection into the reservoir, these particles, possessing amphiphilic properties, can autonomously diffuse within the aqueous

phase toward the interface between crude oil and water, thereby facilitating oil-seeking behavior.

3.3.2. Emulsification Ability of 3NSI16W Particles.
The aging process of emulsions stabilized by different types of SiO_2 particles is depicted in Figure 11. It can be observed that HOSIOH particles initially have a certain emulsification capability with an initial EI value of 82.42%. However, their emulsion stability is poor, and after 1 h, the EI value drops to 21.7%, reaching complete demulsification (EI value of 0) after 7 days. This is because HOSIOH particles have a superhydrophilic structure and tend to adsorb in the water phase.[29] In contrast, 16WSI16W particles exhibit even lower emulsion stability, with the EI value of emulsions stabilized by these particles dropping from an initial 100% to 0 after just 1 h of aging. This is attributed to the strong lipophilicity of 16WSI16W particles, causing them to preferentially adsorb in the oil phase.[30] On the other hand, 3NSI16W particles demonstrate exceptional emulsion stability, with the EI value of emulsions stabilized by them remaining above 60% after 7 days. This is due to the amphiphilic nature of 3NSI16W particles, which enhances the mechanical barrier mechanism of Pickering emulsions.[31] This demonstrates that 3NSI16W particles have the ability to carry oil along with water,
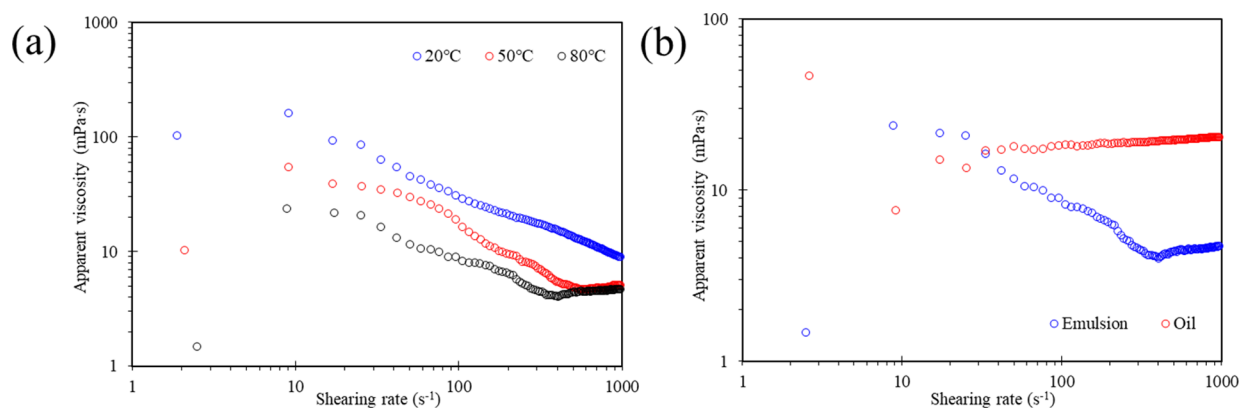
Figure 13. (a) Viscosity changes of emulsions prepared with 3NSI16W particles as a function of temperature. (b) Comparison of the viscosity of emulsions prepared with 3NSI16W particles and crude oil at 80 °C.
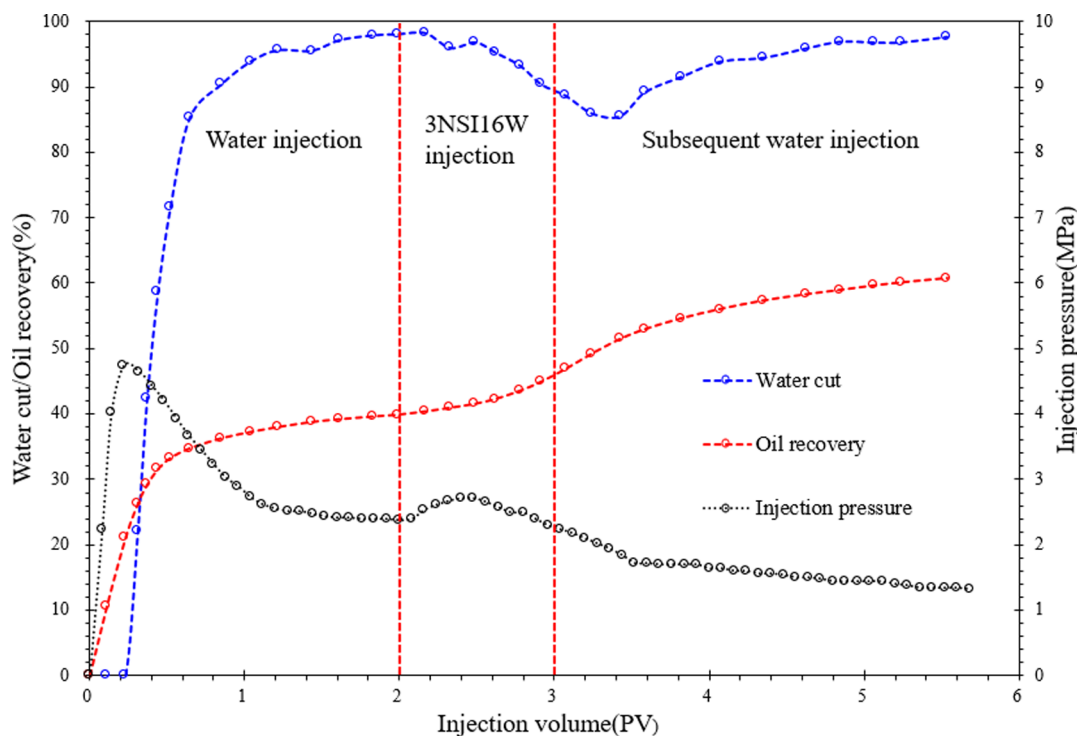

Figure 14. Displacement performance of the 3NSI16W particle dispersion fluid.

effectively "pulling" oil droplets and facilitating their movement within the reservoir.

Figure 12a shows the particle size of emulsions stabilized by 3NSI16W particles at different salt concentrations after aging for 7 days. Emulsions without salt had significantly larger average particle sizes. Emulsions with salt concentrations of 10,000 and 30,000 ppm have similar average particle sizes, which are lower than those without salt. Emulsions with a salt concentration of 50,000 ppm have the smallest average particle size, indicating more stable emulsions.[32] This is because NaCl, as an electrolyte, can shield the surface charges of particles, reducing the energy barrier for particles to adsorb at the oil–water interface. Additionally, it decreases the repulsive forces between particles, facilitating the interface adsorption of 3NSI16W particles and the formation of a dense particle film. This, in turn, enhances the stability of Pickering emulsions.[33] Figure 12b demonstrates that the EI value of emulsions stabilized by 3NSI16W particles remains relatively stable with increasing aging time, with the

highest amplitude being 3.8% for a salt concentration of 50,000 ppm. As the salt concentration increases, the EI value of emulsions stabilized by 3NSI16W particles also increases, indicating stronger stability with higher salt concentrations. This proves that 3NSI16W particles possess high salt resistance and can be effective in highly mineralized reservoirs.

Figure 13a presents the rheological performance of emulsions stabilized by 3NSI16W particles at temperatures of 20 °C (wellhead temperature), 50 °C (casing temperature), and 80 °C (reservoir temperature). The emulsion stabilized by 3NSI16W particles exhibits shear-thickening at low shear rates, followed by shear-thinning as the shear rate increases, demonstrating pseudoplastic fluid characteristics when the shear rate is greater than 10 s^{-1}. As the temperature increases, the viscosity of the emulsion decreases and a second flow region appears. This is due to the increase in temperature causing the long alkyl chains on SiO$_2$ to transform from an ordered to a disordered state, reducing the thickness and density of the solvent coating layer,

and simultaneously decreasing the van der Waals attraction between the particles.[34−36] Figure 13b demonstrates the viscosity of crude oil and emulsion stabilized by 3NSI16W particles at 80 °C. The crude oil shear-thinned at a low shear rate, then underwent shear-thickening, and finally the viscosity stabilized, with the characteristics of an approximate Newtonian fluid. When the shear rate exceeds 27 s^{-1}, the emulsion viscosity stabilized by 3NSI16W particles is lower than the viscosity of crude oil, which can reduce the flow resistance of the oil phase, modify the oil−water mobility ratio, and is conducive to the recovery of crude oil and the enhancement of the displacement efficiency.

3.3.3. Displacement Performance of 3NSI16W Particles. Figure 14 illustrates the displacement performance of 3NSI16W particles in a dispersion fluid. During the initial water injection phase, the introduction of fluids into the rock matrix encounters significant permeability resistance, leading to a rapid surge in the injection pressure. As the water flooding process progresses, the water saturation in the pore media increases. Upon breakthrough, when the injection end communicates with the outlet end, the injection pressure reaches its peak. During the prebreakthrough stage, water flooding mainly plays the role of oil replacement, establishing flow channels within the reservoir. Following the breakthrough, injected water communicates between the inlet and outlet of the rock formation, coexisting as a continuous phase within the porous media. Pressure depletion occurs rapidly, accompanied by a sharp increase in the water content. Although the displacement efficiency of water displacing oil continues to increase slowly after the breakthrough, the water displacement efficiency gradually declines.

During the initial phase of 3NSI16W particle injection, the self-aggregation of particles can plug pore throats, elevate injection pressure, increase the microscopic sweep efficiency, and reduce the water content. As the 3NSI16W particles migrate, they spontaneously move toward the oil−water interface, altering the contact relationship between the two phases, thereby reducing the oil-phase flow resistance and causing a decrease in injection pressure.

Influenced by the oil/water mobility ratio, the water saturation continues to decrease, forming an oil barrier. This effect persists into the subsequent water flooding stage, and when the injection volume reaches 3.4 PV, the water content reaches its minimum level. Subsequently, the remaining oil saturation decreases, leading to an increase in internal core water content, and oil displacement efficiency declines, initiating a phase where water content begins to rise again.

Overall, the 3NSI16W particles increased the oil recovery rate by 20.8%, increasing the effective time of action and the duration of the water content decline. Subsequent water drive phases relied on residual drag coefficients to increase the microscopic ripple coefficient and modified oil−water mobility ratios to increase the degree of sustained recovery.

4. CONCLUSIONS

1. Initially, Janus nano-SiO$_2$ was successfully prepared by the Pickering emulsion interface protection method, and the morphology of strawberry-like intermediate particle HOSI-PW proves that the preparation method is efficient. Structural characterization revealed a distinct asymmetric structure and notable temperature resistance in Janus nanoscale SiO$_2$, showcasing its potential in 150 °C-180 °C high-temperature reservoirs.

2. Janus nano-SiO$_2$ has an excellent ability to enhance the oil−water interface interaction and modify the oil−water mobility ratio. Compared with homogeneous nano-SiO$_2$, Janus nano-SiO$_2$ shows the ability to migrate to the oil−water interface due to its amphiphilicity and excellent emulsion stability for more than 7 days of stable emulsion. At the same time, the Janus nano-SiO$_2$ stable emulsion shows the ability to resist 50000 ppm of high salt, and its viscosity is 5 mPa·s at 80 °C, which is significantly lower than that of the oil phase, effectively reducing the oil phase flow resistance and modifying the oil−water mobility ratio.

3. Flow resistance experiments indicate that during subsequent water flooding processes, the injection pressure increased from 0.023 MPa in the primary water flooding stage to 0.039 MPa. Janus nano-SiO$_2$ can improve the resistance to water flow in the pore channel and increase the sweep efficiency. Displacement test results show that the dispersed Janus nanoscale SiO$_2$ system can increase the crude oil recovery by 20.8%. This can be attributed to its interfacial stability, oil-seeking properties, emulsion stability, and capability to modify the oil−water mobility ratio.

All of these results suggest that Janus nano-SiO$_2$ holds the potential to enhance the extraction efficiency of oil fields characterized by high water content and strong heterogeneity, particularly in environments with elevated temperatures and salinity. This could have significant implications for the oil field industry.

■ AUTHOR INFORMATION

Corresponding Authors

Miaomiao Hu − *School of Chemical Engineering and Technology, Tianjin University, Tianjin 300350, China; Zhejiang Institute of Tianjin University, Shaoxing, Zhejiang 312300, China;* orcid.org/0000-0002-1241-7167; Email: mmhu1990@tju.edu.cn

Jintang Guo − *School of Chemical Engineering and Technology, Tianjin University, Tianjin 300350, China; Zhejiang Institute of Tianjin University, Shaoxing, Zhejiang 312300, China;* Email: jtguo@tju.edu.cn

Authors

Long Zang − *School of Chemical Engineering and Technology, Tianjin University, Tianjin 300350, China*

Jie Cao − *School of Chemical Engineering and Technology, Tianjin University, Tianjin 300350, China*

Yun Cheng − *School of Chemical Engineering and Technology, Tianjin University, Tianjin 300350, China*

Pengpeng Li − *School of Chemical Engineering and Technology, Tianjin University, Tianjin 300350, China*

Hang Zhang − *School of Chemical Engineering and Technology, Tianjin University, Tianjin 300350, China*

Complete contact information is available at:
https://pubs.acs.org/10.1021/acsomega.4c00317

Notes

The authors declare no competing financial interest.

REFERENCES

(1) Wei, B.; Nie, X.; Zhang, Z.; Ding, J.; Shayireatehan, R.; Ning, P.; Deng, D.; Cao, Y. Productivity Equation of Fractured Vertical Well with Gas−Water Co-Production in High-Water-Cut Tight Sandstone Gas Reservoir. *Processes* **2023**, *11* (11), 3123.

(2) Zhao, M.; Xin, X.; Yu, G.; Hu, R.; Gong, Y. Mechanistic Study and Optimization of High Water Cut Phase Management Strategies in Fracture-Vuggy Carbonate Reservoirs with Bottom Water. *Processes* [Online] **2023**, *11* (11), 3135.

(3) Xue, L.; Liu, P.; Zhang, Y. Status and Prospect of Improved Oil Recovery Technology of High Water Cut Reservoirs. *Water* **2023**, *15* (7), 1342.

(4) Alnarabiji, M. S.; Husein, M. M. Application of bare nanoparticle-based nanofluids in enhanced oil recovery. *Fuel* **2020**, *267*, No. 117262.

(5) Hou, J.; Du, J.; Sui, H.; Sun, L. A review on the application of nanofluids in enhanced oil recovery. *Frontiers of Chemical Science and Engineering* **2022**, *16* (8), 1165−1197.

(6) Torsaeter, O. Application of Nanoparticles for Oil Recovery. *Nanomaterials* **2021**, *11* (5), 1063.

(7) Pereira, M. L. D. O.; Maia, K. C. B.; Silva, W. C.; Leite, A. C.; Francisco, A. D. D. S.; Vasconcelos, T. L.; Nascimento, R. S. V.; Grasseschi, D. Fe3O4 Nanoparticles as Surfactant Carriers for Enhanced Oil Recovery and Scale Prevention. *ACS Applied Nano Materials* **2020**, *3* (6), 5762−5772.

(8) Ehtesabi, H.; Ahadian, M. M.; Taghikhani, V.; Ghazanfari, M. H. Enhanced Heavy Oil Recovery in Sandstone Cores Using TiO2 Nanofluids. *Energy Fuels* **2014**, *28* (1), 423−430.

(9) Zargar, G.; Arabpour, T.; Manshad, A. K.; Ali, J. A.; Sajadi, S. M.; Keshavarz, A.; Mohammadi, A. H. Experimental investigation of the effect of green TiO2/Quartz nanocomposite on interfacial tension reduction, wettability alteration, and oil recovery improvement. *Fuel* **2020**, *263*, No. 116559.

(10) Chaudhury, M. K. Complex fluids - Spread the word about nanofluids. *Nature* **2003**, *423* (6936), 131−132.

(11) Li, Y.; Kong, B.; Zhang, W.; Bao, X.; Jin, J.; Wu, X.; Guo, Y.; Liu, Y.; Wang, Y.; He, X.; Zhang, H.; Shen, Z.; Sha, O. Field Application of Alkali/Surfactant/Polymer Flood with Novel Mixtures of Anionic/Cationic Surfactants for High-Temperature and High-Water-Cut Mature Sandstone Reservoir. *SPE Reservoir Evaluation & Engineering* **2020**, *23* (03), 1093−1104.

(12) Jia, H.; Wang, D.; Wang, Q.; Dai, J.; Wang, Q.; Wen, S.; Wang, Z.; Wang, B.; Jiang, X.; Li, X.; Lv, K. The synthesis of novel amphiphilic GOJS-Cn nanoparticles and their further application in stabilizing pickering emulsion and enhancing oil recovery. *J. Pet. Sci. Eng.* **2022**, *214*, No. 110537.

(13) Fernandez-Rodriguez, M. A.; Song, Y.; Rodríguez-Valverde, M. A.; Chen, S.; Cabrerizo-Vilchez, M. A.; Hidalgo-Alvarez, R. Comparison of the Interfacial Activity between Homogeneous and Janus Gold Nanoparticles by Pendant Drop Tensiometry. *Langmuir* **2014**, *30* (7), 1799−1804.

(14) Tang, S.; Sun, Z.; Dong, Y.; Zhu, Y.; Hu, H.; Wang, R.; Liao, H.; Dai, Q. Preparation of Amphiphilic Janus-SiO2 Nanoparticles and Evaluation of the Oil Displacement Effect. *ACS Omega* **2024**, *9* (5), 5838−5845.

(15) Hong, L.; Jiang, S.; Granick, S. Simple method to produce Janus colloidal particles in large quantity. *Langmuir* **2006**, *22* (23), 9495−9499.

(16) Jeelani, P. G.; Mulay, P.; Venkat, R.; Ramalingam, C. Multifaceted Application of Silica Nanoparticles. A Review. *Silicon* **2020**, *12* (6), 1337−1354.

(17) Delon, T.; Parsai, T.; Kilic, U.; Schubert, M.; Morin, S. A.; Li, Y. Impacts of particle surface heterogeneity on the deposition of colloids on flat surfaces. *Environmental Science: Nano* **2021**, *8* (11), 3365−3375.

(18) Cao, B.; Xie, K.; Lu, X.; Cao, W.; He, X.; Xiao, Z.; Zhang, Y.; Wang, X.; Su, C. Effect and mechanism of combined operation of profile modification and water shutoff with in-depth displacement in high-heterogeneity oil reservoirs. *Colloids Surf., A* **2021**, *631*, No. 127673.

(19) Jie, C.; Hu, M.; Zang, L.; Li, P.; Zhang, H.; Cheng, Y.; Guo, J. Design of low-consumption epoxy resin porous plugging material via emulsification-curing method. *Colloids Surf., A* **2024**, *680*, No. 132669.

(20) Jia, H.; Wu, H. Y.; Wei, X.; Han, Y. G.; Wang, Q. X.; Song, J. Y.; Dai, J. J.; Yan, H.; Liu, D. X. Investigation on the effects of AlOOH nanoparticles on sodium dodecylbenzenesulfonate stabilized o/w emulsion stability for EOR. *Colloids and Surfaces a-Physicochemical and Engineering Aspects* **2020**, *603*, No. 125278.

(21) A'Yuni, Q.; Rahmayanti, A.; Hartati, H.; Purkan, P.; Subagyo, R.; Rohmah, N.; Itsnaini, L. R.; Fitri, M. A. Synthesis and characterization of silica gel from Lapindo volcanic mud with ethanol as a cosolvent for desiccant applications. *RSC Adv.* **2023**, *13* (4), 2692−2699.

(22) Liu, X. Y.; Fu, Z. Y.; Zhang, F. D.; Wu, M.; Dong, Y. M. Synthesis of silica Janus nanosheets and their application to the improvement of interfacial interaction in wood polymer composites. *Journal of Materials Research and Technology-Jmr&T* **2021**, *15*, 4652−4661.

(23) Jia, H.; Dai, J. J.; Miao, L. C.; Wei, X.; Tang, H. T.; Huang, P.; Jia, H. D.; He, J.; Lv, K. H.; Liu, D. X. Potential application of novel amphiphilic Janus-SiO2 nanoparticles stabilized O/W/O emulsion for enhanced oil recovery. *Colloids and Surfaces a-Physicochemical and Engineering Aspects* **2021**, *622*, No. 126658.

(24) Gorbunov, D.; Nenasheva, M.; Naranov, E.; Maximov, A.; Rosenberg, E.; Karakhanov, E. Tandem hydroformylation/hydrogenation over novel immobilized Rh-containing catalysts based on tertiary amine-functionalized hybrid inorganic-organic materials. *Applied Catalysis A: General* **2021**, *623*, No. 118266.

(25) Gautier, F.; Destribats, M.; Perrier-Cornet, R.; Dechezelles, J. F.; Giermanska, J.; Heroguez, V.; Ravaine, S.; Leal-Calderon, F.; Schmitt, V. Pickering emulsions with stimulable particles: from highly- to weakly-covered interfaces. *Phys. Chem. Chem. Phys.* **2007**, *9* (48), 6455−6462.

(26) Skoczylas, M.; Bocian, S.; Buszewski, B. Influence of silica functionalization by amino acids and peptides on the stationary phases zeta potential. *Journal of Chromatography A* **2018**, *1573*, 98−106.

(27) Wang, C.; Jiang, H.; Li, Y. Water-in-oil Pickering emulsions stabilized by phytosterol/chitosan complex particles. *Colloids Surf., A* **2023**, *657*, No. 130489.

(28) Zhang, Y.; You, Q.; Fang, J. C.; Liu, Y. F.; Gao, M. W.; Fan, H. F.; Dai, C. L. Preparation and Performance Evaluation of Fatty Amine Polyoxyethylene Ether Diethyl Disulfonate for Enhanced Oil Recovery in High-Temperature and High-Salinity Reservoirs. *J. Surfactants Deterg.* **2018**, *21* (4), 489−496.

(29) Binks, B. P.; Rodrigues, J. A. Double inversion of emulsions by using nanoparticles and a di-chain surfactant. *Angew. Chem., Int. Ed.* **2007**, *46* (28), 5389−5392.

(30) Binks, B. P. Particles as surfactants - similarities and differences. *Curr. Opin. Colloid Interface Sci.* **2002**, *7* (1−2), 21−41.

(31) Mao, X. H.; Yang, D. L.; Xie, L.; Liu, Q.; Tang, T.; Zhang, H.; Zeng, H. B. Probing the Interactions between Pickering Emulsion Droplets Stabilized with pH-Responsive Nanoparticles. *J. Phys. Chem. B* **2021**, *125* (26), 7320−7331.

(32) Hou, Y. J.; Li, Y. M.; Wang, L. S.; Chen, D. F.; Bao, M. T.; Wang, Z. N. Amphiphilic Janus particles for efficient dispersion of oil contaminants in seawater. *J. Colloid Interface Sci.* **2019**, *556*, 54−64.

(33) Sharma, T.; Kumar, G. S.; Chon, B. H.; Sangwai, J. S. Thermal stability of oil-in-water Pickering emulsion in the presence of nanoparticle, surfactant, and polymer. *Journal of Industrial and Engineering Chemistry* **2015**, *22*, 324−334.

(34) Cui, S.-M.; Hashmi, S.; Li, W.-Q.; Handschuh-Wang, S.; Zhu, C.-T.; Wang, S.-C.; Huang, Y.-F.; Zhu, G.-M.; Stadler, F. J. Rheology of graphene oxide stabilized Pickering emulsions. *Soft Matter* **2023**, *19* (24), 4536−4548.

(35) Farias, B. V.; Brown, D.; Hearn, A.; Nunn, N.; Shenderova, O.; Khan, S. A. Nanodiamond-stabilized Pickering emulsions: Microstructure and rheology. *J. Colloid Interface Sci.* **2020**, *580*, 180−191.

(36) Brown, N.; de la Pena, A.; Razavi, S. Interfacial rheology insights: particle texture and Pickering foam stability. *J. Phys.: Condens. Matter* **2023**, *35* (38), 384002.